

# Role of interfacial elasticity of microemulsions on the morphology of TiO<sub>2</sub> nanostructures: stiff templates versus flexible templates

Paula V. Messina · Valeria Verdinelli · Olga Pieroni ·  
Juan Manuel Ruso

Received: 22 June 2012 / Revised: 27 August 2012 / Accepted: 28 August 2012

© Springer-Verlag 2012

**Abstract** The effects of temperature and interfacial elasticity on nanostructured titanium dioxide (TiO<sub>2</sub>) microemulsions templated materials have been investigated. The aim was to establish a simple and rapid selection of the best experimental conditions for achieving some required material property. TiO<sub>2</sub> materials have been prepared through reactive microemulsion precipitation. The effect of microemulsion process parameters (temperature and oil phase density) on the final material characteristics has been investigated. The titania nanopowders were characterized by X-ray diffraction, Fourier transform infrared spectroscopy, field emission scanning electron microscopy, and N<sub>2</sub> adsorption–desorption isotherms. The results obtained by different process conditions show that the nonpolar phase density and temperature of microemulsions have a great influence on the final characteristics of the obtained material. A reduction of the microemulsion oil density causes a significant decrease in the particle agglomeration and an augment of the material-specific surface area and pore volume. At the same time, rutile is favored over anatase phase. The increase of template microemulsion temperature produces, in some systems, a morphology change from granular to a bicontinuous structure.

**Keywords** Microemulsions · Templates · Titanium dioxide · Nanostructures · Interfacial elasticity

---

P. V. Messina · V. Verdinelli · O. Pieroni  
Departamento de Química, Universidad Nacional del Sur,  
CONICET-INQUISUR,  
8000 Bahía Blanca, Argentina

J. M. Ruso (✉)  
Soft Matter and Molecular Biophysics Group, Facultad de Física,  
Universidad de Santiago de Compostela,  
15782 Santiago de Compostela, Spain  
e-mail: juanm.ruso@usc.es

## Introduction

Nanomaterials have been attracting extensive attention because of their unique and often improved mechanical, electrical, optical, and chemical properties as compared with conventional polycrystalline materials [1–4]. Titanium dioxide (TiO<sub>2</sub>) is a very useful semiconducting transition metal oxide and exhibits unique characteristics such as low cost, easy handling, nontoxic, high gas sensitivity and dielectric constant, resistance to photochemical and chemical erosion, and chemical and photocatalyzing properties [5]. These advantages cause TiO<sub>2</sub> materials to be widely investigated for various applications in photocatalysis, photovoltaic cells, photonic crystals, sensors, ultraviolet blockers, smart surface coatings, pigments, and paints [6–10]. To date, many efforts have been made to prepare nanocrystalline TiO<sub>2</sub>. Numerous techniques including plasma processes, sol–gel, synthesis in supercritical fluids, chemical precipitation methods, hydrothermal crystallization, and chemical vapor deposition [11] have been employed. These methods suffer the problem of extreme reaction conditions.

Consequently, there is a strong social and economic pressure that encourages the design of cheaper and more sustainable materials, products, and processes [12]. The self-assembly of relatively small molecules yielding new nano-objects opens unforeseen and unique opportunities for a variety of fields in science as well as for several industries. A number of commercial products based on nanostructures are already currently available for public consumption [13]. For instance, architecturally complex assemblies and tailored functionalized polymers have been specifically employed in sensors, semiconductors, and pharmaceuticals devices [14–16]. Mixtures of different molecules which self-assemble in aqueous solution represent an interesting alternative for the design of nanoparticles due to its higher flexibility when compared to systems based on

homogeneous molecules. The competition between electrostatic interactions favoring the mixing and hydrophobic, promoting segregation, may result in modulated phases or two-dimensional self-assembly. This has been suggested as a tactic in different biological systems [17–20].

In this sense, reverse microemulsion synthesis of oxide materials has been shown to be a very promising procedure for obtaining ultrafine and nanometric particles with controlled size and shape. The main idea behind this technique is that by appropriate control of the synthesis parameters, one can use these nanoreactors to generate tailor-made products down to a nanoscale level with new and special properties. Despite the several investigations that have been carried out on this synthesis route in the last years [21–24], the process control is not well established, probably due to the complexity of the microemulsion employed in the particles' development. The literature on this processing route suffers from the lack of studies on the influence of microemulsion parameters on the characteristics of the final synthesized powder products.

The shape (and size) of the dispersed nanodroplet in a microemulsion is mainly governed by the curvature free energy and is determined by film elasticity [25–27]. The elasticity of the film depends not only on the surfactant type [28] and the thermodynamic conditions but also on the nature of the oil phase [29].

In a previous work, we obtained silica-based materials of different size and morphology by varying water-to-surfactant microemulsion ratio. We found that granular material became a bicontinuous system with the augment of microemulsion water content. The effect of this parameter on the material adsorption properties was also investigated [23]. Here, we try to extend the above studies to evaluate the effect of microemulsion temperature and oil phase density on nanostructured TiO<sub>2</sub> material properties. In this work, we have used six different microemulsion systems to synthesize nanostructured TiO<sub>2</sub> materials. The variations of microemulsion nonpolar phase and temperature were correlated with the size, shape, and crystal structure of the obtained materials.

## Experimental

### Materials and samples

Sodium bis(2-ethylhexyl) sulfosuccinate (Aerosol OT (AOT), 99 % Sigma), *n*-hexane (Merck,  $\delta=0.6548 \text{ g cm}^{-3}$ ), *n*-heptane (Merck,  $\delta=0.684 \text{ g cm}^{-3}$ ), cyclohexane (Merck,  $\delta=0.776 \text{ g cm}^{-3}$ ), and TiCl<sub>4</sub> (Carlo Erba, 99 %,  $\delta=1.722 \text{ g cm}^{-3}$ ) were used without further purification. For microemulsion preparation, only triple-distilled water was used.

### Microemulsion systems

Experiments were performed on water/AOT/alkane microemulsion systems, for the alkanes *n*-hexane, *n*-heptane, and cyclohexane. The composition of the microemulsion is given here in terms of  $W_0$ , the ratio of water to surfactant molar concentrations, and  $S_0$ , the ratio of oil to surfactant molar concentration. Microemulsion systems of  $S_0=30$  and  $W_0=60$  were prepared. In the AOT microemulsion system,  $W_0$  essentially determines the radius of the water droplets and  $S_0$  their concentration in the oil phase [30] (for a given  $W_0$ , the droplet concentration is proportional to  $1/S_0$ ). As the critical micellization concentration of AOT in both oil and water is low compared with the concentration used here, it can be assumed that all the surfactant molecules are localized at the interface between water and oil [31]. The microemulsions were prepared using the injection method, by mixing an appropriate quantity of water with an AOT solution in oil [32]. The resulting microemulsions were placed in Teflon-stoppered test tubes and left to equilibrate for 24 h at the desired temperature conditions (30 and 40 °C) before used.

We worked within the boundaries of the L2 phase, where the structure of the aggregates is spherical [33]. This droplet structure has been found to be fairly insensitive to the concentration of the droplets. Following the above procedure, six different microemulsion systems were prepared: (I) water/AOT/*n*-hexane, 30 °C; (II) water/AOT/*n*-heptane, 30 °C; (III) water/AOT/cyclohexane, 30 °C; (IV) water/AOT/*n*-hexane, 40 °C; (V) water/AOT/*n*-heptane, 40 °C; and (VI) water/AOT/cyclohexane, 40 °C.

### Microemulsion-mediated hydrothermal synthesis of TiO<sub>2</sub> samples

Titanium oxides structures (TiO<sub>2</sub>) were prepared using a combination of a microemulsion-mediated hydrothermal synthesis: 1.4 mL of TiCl<sub>4</sub> was added to 15 mL of each of the above-described microemulsion and left 3 days to react following the reaction shown below:



Then, HCl and the nonpolar solvent were eliminated by evaporation under vacuum. The resulting gel was left for 24 h in an autoclave at 100 °C. The obtained materials were filtered and washed with triple-distilled water and left to dry at room temperature. Finally, it was calcined for 7 h at 540 °C in an air flux. The obtained materials were called M<sub>I</sub>, M<sub>II</sub>, M<sub>III</sub>, M<sub>IV</sub>, M<sub>V</sub>, and M<sub>VI</sub>; the suffixes correspond to the microemulsion system used as template.

## Methods

Field emission scanning electron microscopy

Field emission scanning electron microscopy (FE-SEM) was performed using a JEOL 35 CF (Tokyo, Japan).

X-ray powder diffraction

Powder X-ray diffraction (XRD) data were collected with a Philips PW 1710 diffractometer with Cu-K $\alpha$  radiation ( $\lambda = 1.5418 \text{ \AA}$ ) and graphite monochromator operated at 45 kV, 30 mA, and 25 °C.

Fourier transform infrared spectroscopy spectroscopy

Fourier transform infrared spectroscopy (FT-IR) experiments were done in a Nicolet FT-IR Nexus 470 Spectrophotometer. To avoid coadsorbed water, the samples were dried under vacuum until constant weight was achieved and diluted with KBr powder before the FT-IR spectra were recorded.

Nitrogen adsorption–desorption isotherms

The nitrogen isotherms at  $-196 \text{ }^\circ\text{C}$  were measured with a Micrometrics Model Accelerated Surface Area and Porosimetry System 2020 instrument. Each sample was degassed at  $100 \text{ }^\circ\text{C}$  for 720 min at a pressure of  $10^{-4} \text{ Pa}$ .

## Results

Morphology and particle size

Scanning electron microphotographs of  $M_I$ ,  $M_{II}$ , and  $M_{III}$  materials calcined at  $540 \text{ }^\circ\text{C}$  are shown in Fig. 1. The particles of these materials have spherical morphology. In addition, the size and degree of association increase with increasing the template microemulsion nonpolar phase density. Apparently, discernible pores are present between the nanosized  $\text{TiO}_2$  particles. The pores can be seen as black spots with nonordered wormhole-like structures, whereas the nanosized  $\text{TiO}_2$  particles appear white. The effect of temperature on the synthesized materials can be appreciated from inspection of Fig. 2, where it can be observed how the systems templated with water/AOT/*n*-hexane and water/AOT/cyclohexane microemulsions undergo changes from granular to a bicontinuous phase. For those materials prepared from water/AOT/*n*-heptane microemulsion, an increase of particle association is observed, but without forming a bicontinuous structure.

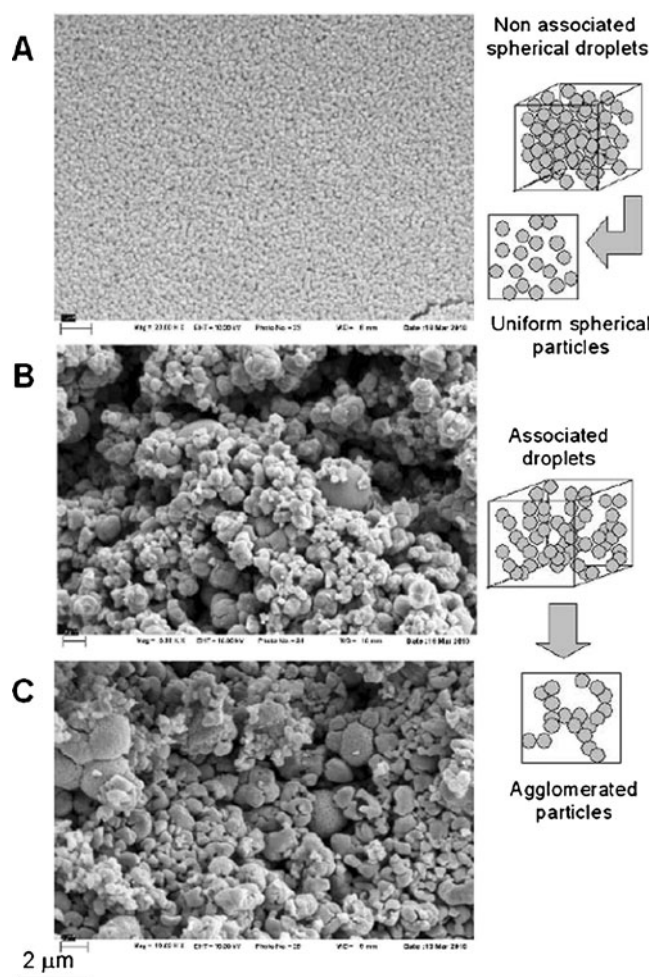


**Fig. 1** FE-SEM microphotographs showing the surface morphology of  $\text{TiO}_2$  samples prepared by reverse microemulsions: **a**  $M_I$ , **b**  $M_{II}$ , and **c**  $M_{III}$

Also, fractal dimension can be obtained from SEM images of the gels. To do this, the box counting method was applied to different SEM images. This protocol consists of applying an increasingly fine grid over the area studied and in counting at each iteration the number of boxes containing at least one part of the object to be measured. The fractal dimension  $D_f$  is then linked to the number  $n(s)$  of boxes of dimension  $s$  necessary to fill the surface area of the particle according to [34]:

$$D_f = \lim_{s \rightarrow 0} \frac{\ln n(s)}{\ln \left(\frac{1}{s}\right)} \quad (1)$$

This method was also optimized by means of a calculation procedure stemming from the work of Foroutan-Pour et al. [35], which allows a precise determination of the key parameters of the method, namely, the number and the dimensions of the boxes [36]. The images, initially with 256 gray levels and  $1,024 \times 768$  pixels in size, are converted to binary images. The

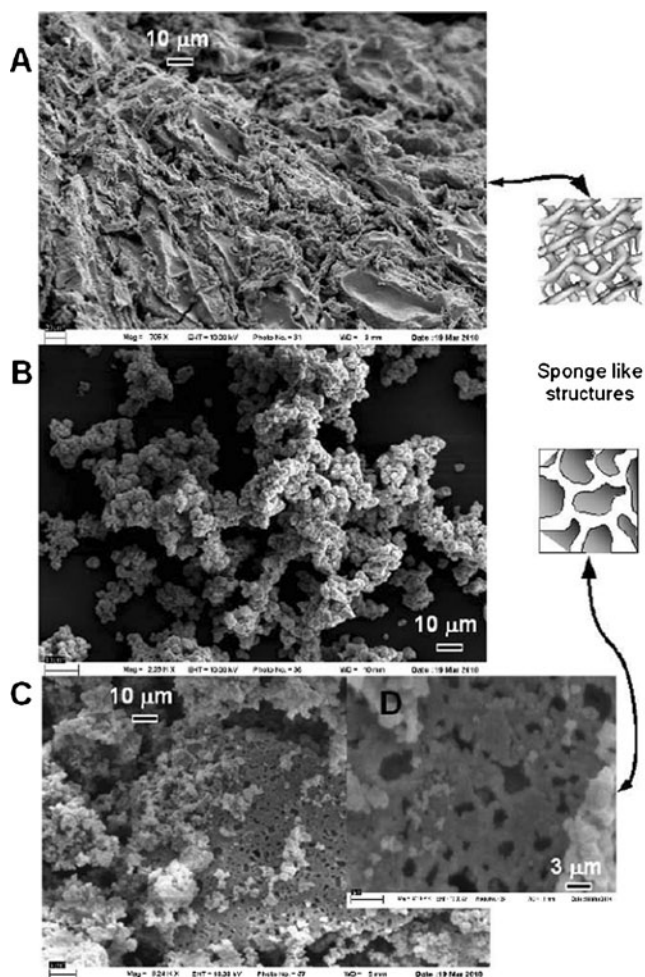


**Fig. 2** FE-SEM microphotographs showing the surface morphology of TiO<sub>2</sub> samples prepared by reverse microemulsions: **a** M<sub>IV</sub>, **b** M<sub>V</sub>, and **c** M<sub>VI</sub>

fractal dimension is then derived from the slope of a least-square linear fit of the plot of  $\log n$  versus  $\log$  (box size), where  $n$  is the number of nonoverlapping equal boxes that would fill the projected surface area of the aggregate. This operation can be carried out by different software packages [37]. Log–log representations for the calculations of fractal dimension on systems under study lead to the values listed in Table 1. It is interesting to see how the fractal dimension tends to decrease as oil density increases. This fact can be observed for both temperatures. Previous studies have analyzed the effect of type of oil on the particle size showing that the

**Table 1** Fractal dimension of the synthesized materials obtained from analysis of SEM images

Microemulsion template system	30 °C	40 °C
Water/AOT/ <i>n</i> -hexane	1.84	1.80
Water/AOT/ <i>n</i> -heptane	1.87	1.70
Water/AOT/cyclohexane	1.77	1.65

particle size decreases with decreasing oil density [38]. However, to the best of our knowledge, this is the first study where the fractal dimension of the materials is related to the interfacial elasticity of the templates.

#### XRD and FT-IR analysis

Figures 3 and 4 show the XRD patterns of all tested materials. The nanopowders exhibit a high degree of crystallinity. Relatively broad diffraction peaks due to TiO<sub>2</sub> (anatase and rutile) structures are present in all synthesized materials. No obvious peaks are observed regarding brookite ((121), at  $2\theta=30.8^\circ$ ), some peaks that correspond to TiO, Ti<sub>5</sub>O<sub>9</sub>, and Ti<sub>7</sub>O<sub>3</sub> appear too, but they are negligible. The average crystallite size ( $L$ ) was determined by XRD line broadening technique using the Debye–Scherrer equation:

$$L = \frac{0.94\lambda}{b \cos \theta} \quad (2)$$

where  $\lambda$  is the wavelength of the X-ray used and  $b$  is the relative peak broadening, calculated as  $b^2 = b_{\text{exp}}^2 - b_{\text{ref}}^2$ ,

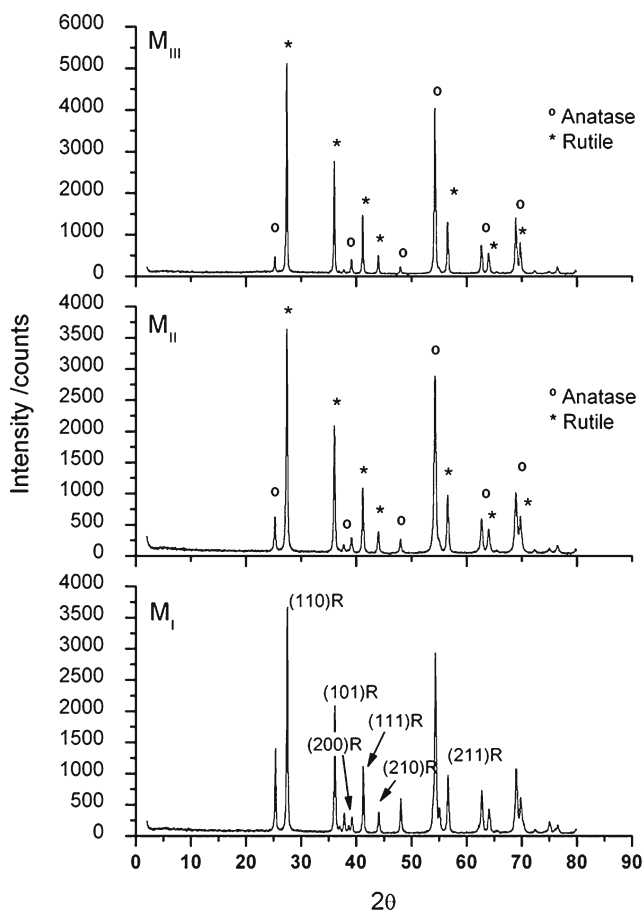


**Fig. 3** XRD pattern of TiO<sub>2</sub> nanopowders obtained through precipitation in microemulsion after calcination at 540 °C for 7 h in air flux: M<sub>I</sub> (water/AOT/*n*-hexane, 30 °C), M<sub>II</sub> (water/AOT/*n*-heptane, 30 °C), and M<sub>III</sub> (water/AOT/cyclohexane, 30 °C). R rutile

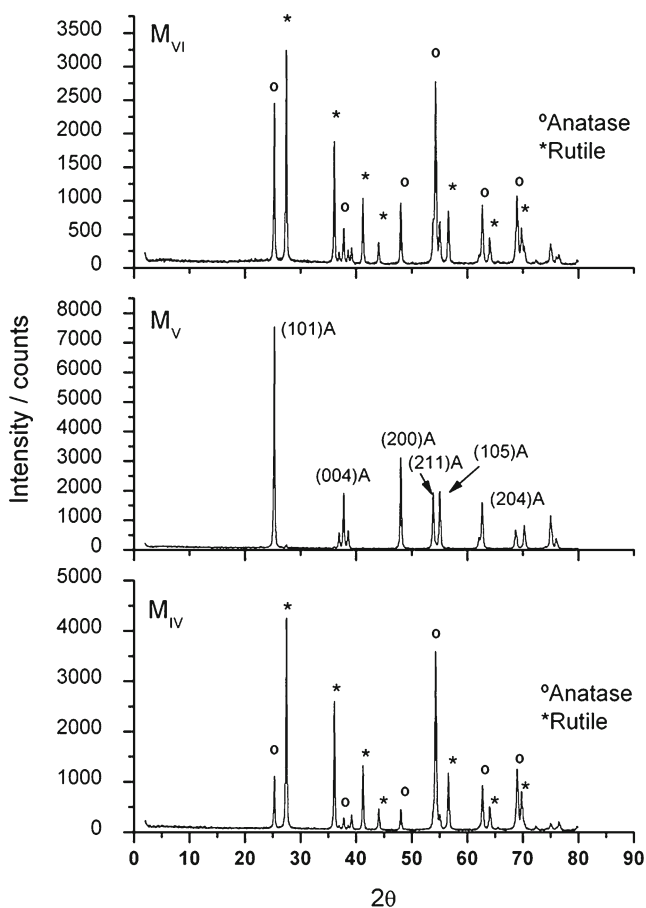


**Fig. 4** XRD pattern of TiO<sub>2</sub> nanopowders obtained through precipitation in microemulsion after calcination at 540 °C for 7 h in air flux: *M<sub>VI</sub>* (water/AOT/*n*-hexane, 40 °C), *M<sub>V</sub>* (water/AOT/*n*-heptane, 40 °C), and *M<sub>IV</sub>* (water/AOT/cyclohexane, 40 °C). A anatase

where  $b_{\text{exp}}$  and  $b_{\text{ref}}$  are half widths at maxima observed on a given sample and on a reference material which is ideally crystalline, respectively [39]. Results are shown in Table 2.

Changes in temperature conditions or in the oil phase during template emulsion preparation result in an alteration of TiO<sub>2</sub> crystalline phase. Table 2 presents the rutile-to-anatase ratio ( $F_r$ ) computed for each material from the XRD intensity data by the following equation [40]:

$$F_r = 1 - \left(1 + 1.265 I_{\text{rutile}(110)} / I_{\text{anatase}(101)}\right)^{-1} \quad (3)$$

Materials prepared at 30 °C present a high proportion of rutile phase, and such proportion increases as the oil phase density in the template microemulsion augments. On the other hand, a change in the synthesis temperature conditions favors anatase phase.

The percentage of anatase phase depends on the template microemulsion system. Thus, for the material templated with water/AOT/*n*-hexane microemulsion, the increase of temperature causes a small diminution of rutile phase. When cyclohexane is used instead *n*-hexane, a 30 % plus of anatase phase is observed with the increase of temperature, and for *M<sub>V</sub>* (TiO<sub>2</sub> material templated with water/AOT/*n*-heptane microemulsion, at 40 °C), a single-anatase phase (without rutile) is obtained.

To clarify the state of anatase after crystallization, IR transmission spectra, shown in Figs. 5 and 6, were analyzed for all tested materials before calcinations. The peak appearing near 3,400 cm<sup>-1</sup> is due to stretching vibration of O-H group, while the corresponding peak at 1,628 cm<sup>-1</sup> can be ascribed to bending vibrations of adsorbed water molecules. The peaks appearing near 2,900 and 900–1,300 cm<sup>-1</sup> correspond to organic bonds. Ti-O-Ti appears in region 400–600 cm<sup>-1</sup>, which arises from the lattice vibration of TiO<sub>2</sub> [41]. An increase of adsorption bands due to organic residues can be found in such materials which lead to a major content of rutile phase (*M<sub>I</sub>*, *M<sub>II</sub>*, *M<sub>III</sub>*, *M<sub>IV</sub>*), while much smaller bands are visible in *M<sub>VI</sub>* (major content of anatase phase). For *M<sub>I</sub>* and *M<sub>IV</sub>*, adsorption bands due to H<sub>2</sub>O, OH are also distinguished. No bands related to H<sub>2</sub>O, OH or organic residues can be appreciated for *M<sub>V</sub>* where single anatase phase is obtained.

## N<sub>2</sub> adsorption–desorption analysis

The obtained N<sub>2</sub> adsorption–desorption results for all tested materials are summarized in Table 3. To determine the pore radius ( $r_p$ ) the Kelvin equation was used [42]:

$$k_B T \ln \left( \frac{p}{p_0} \right) = - \frac{2\sigma v \cos \theta}{r_m} \quad (4)$$

where  $k_B$  is the Boltzmann constant,  $T$  is the absolute temperature,  $p$  is the vapor pressure in the gas phase,  $p_0$  is the vapor pressure at saturation onto a flat liquid surface at temperature  $T$ ,  $\sigma$  is the surface tension of the liquid adsorbate,  $r_m$  is the mean radius of curvature of the liquid/gas interface, taken as the pore radius,  $\theta$  is the contact radius, and  $v$  is the volume per molecule of liquid adsorbate. For nitrogen at -196 °C,  $\sigma = 8.88 \text{ mNm}^{-1}$ ,  $\theta = 0$ , and  $v = 0.057589 \text{ nm}^3$  [42]. To determine the Brunauer–Emmet–Teller (BET) area,  $A_{\text{BET}}$ , the nitrogen molecules' diameter is taken as 0.43 nm, calculated by assuming the closest packing spheres [43], and the area per molecule  $a_m = 0.1620 \text{ nm}^2$ .

**Table 2** Textural parameters of prepared TiO<sub>2</sub> samples

Microemulsion template system	30 °C		40 °C	
	$F_r$	$L^a/\text{nm}$	$F_r$	$L^a/\text{nm}$
Water/AOT/ <i>n</i> -hexane	0.79	9.51	0.80	9.77
Water/AOT/ <i>n</i> -heptane	0.88	9.23	0	12.58
Water/AOT/cyclohexane	0.93	12.17	0.62	11.33

$F_r$  rutile fraction,  $L$  average crystalline size

<sup>a</sup> Computed from anatase peak of XRD by line broadening

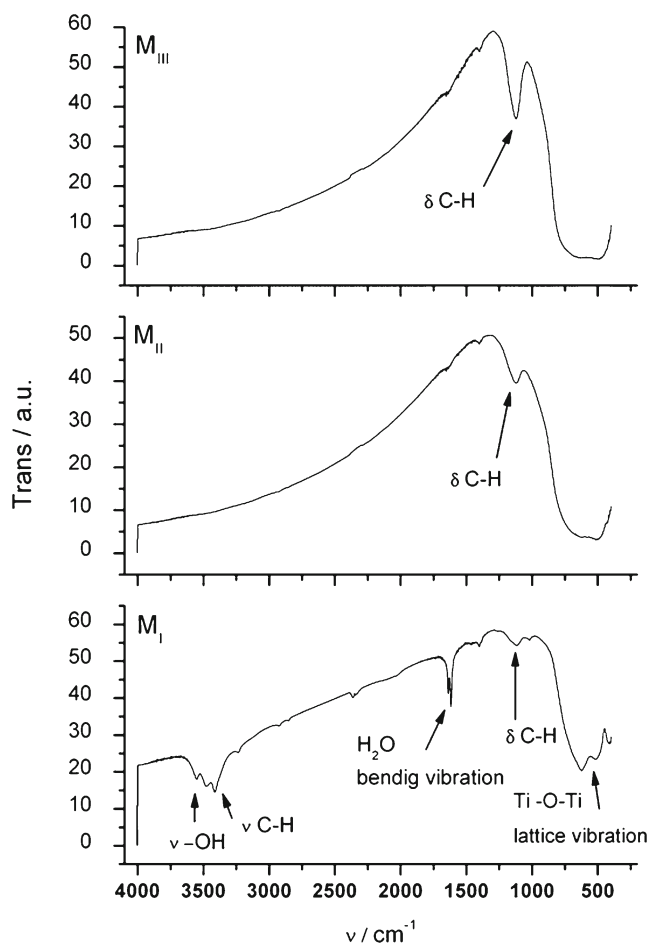


**Fig. 5** FT-IR of TiO<sub>2</sub> samples. *M<sub>I</sub>* (water/AOT/*n*-hexane, 30 °C), *M<sub>II</sub>* (water/AOT/*n*-heptane, 30 °C), and *M<sub>III</sub>* (water/AOT/cyclohexane, 30 °C)

In the so-called modified Kelvin equation, which is the basis of the Barrett–Joyner–Halenda (BJH) method [44], used to extract pore size distribution from the isotherm analysis,  $2/r_m$  is replaced by  $f/(r_p - t)f/(r_p + t)$ , where  $r_p$  is the pore radius,  $f$  is the meniscus shape factor, which, provided there is a perfect wetting, equals 1 or 2 in relation to the filling (adsorption) or the emptying (desorption) of the pore, and  $t$  is the statistical thickness of the adsorption film on a pore wall. The surface layer thickness  $t$  for nitrogen adsorption on silica is given by [45]:

$$t(nm) = 0.1 \left\{ \frac{13.99}{0.034 - \log\left(\frac{p}{p_0}\right)} \right\}^{\frac{1}{2}} \quad (5)$$

From  $t$  plots proposed by Halsey [46], it is possible to determine the total surface area ( $A_{\text{tot}}$ ), the external surface area ( $A_{\text{ext}}$ ), the pore volume ( $V_{\text{tp}}$ ), and the core volume ( $V_c$ ), as explained below. The  $t$  plot of pore structure analysis is based on the assumption that micropore filling in porous solids takes place by the formation of successive layers of the adsorbate until the layers in opposite pore walls merge.

As an example, N<sub>2</sub> adsorption–desorption isotherm,  $t$  plot, and pore radius distribution for *M<sub>I</sub>* are shown in Fig. 7. The  $t$  plot shows the typical appearance presented by adsorbents with slit-shaped pores. Below point “a,” no pores are filled; between a and “b,” mesopores are filled, indicating the minimum pore size; and above “c,” Kelvin capillary condensation occurs. Since the intercept of the straight line at low  $t$  values is not 0, it follows that micropores also are present, whose volume is the intercept, and the slope equals the free surface. Similar results are obtained for the rest of studied materials.

The BET specific area ( $A_{\text{BET}}$ ) of *M<sub>I</sub>*, *M<sub>II</sub>*, and *M<sub>III</sub>* samples is 86.89, 45.89, and 32.18 m<sup>2</sup>g<sup>-1</sup>, respectively. For those materials, the augment of microemulsion alkane phase density results in a diminution of micropore volume ( $V_{\text{spat}}$ ), while it has no significant effect on pore diameter ( $D_{\text{aap}}$ ). The increase of temperature synthesis conditions causes an augment of  $A_{\text{BET}}$  from 45.89 to 119.11 m<sup>2</sup>g<sup>-1</sup> for the material templated with water/AOT/*n*-heptane and from 32.18 to 60.70 m<sup>2</sup>g<sup>-1</sup> for those prepared with water/AOT/cyclohexane microemulsions, while in *M<sub>I</sub>*, it produces a decrease in  $A_{\text{BET}}$  to 62.09 m<sup>2</sup>g<sup>-1</sup>. Similar variations present the parameters  $V_{\text{spat}}$  and  $D_{\text{aap}}$ .

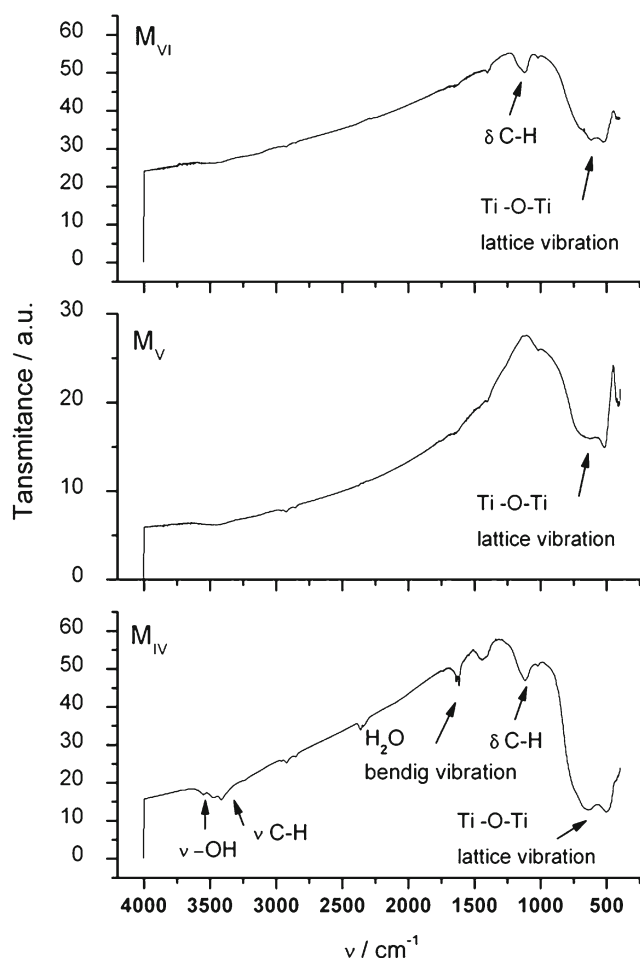


**Fig. 6** FT-IR of TiO<sub>2</sub> samples. *M<sub>IV</sub>* (water/AOT/*n*-hexane, 40 °C), *M<sub>V</sub>* (water/AOT/*n*-heptane, 40 °C), and *M<sub>VI</sub>* (water/AOT/cyclohexane, 40 °C)

**Table 3** Nitrogen adsorption data of the different samples

Sample	$A_{sp}$ (m <sup>2</sup> /g)	$A_{BET}$ (m <sup>2</sup> /g)	$A_{text}$ (m <sup>2</sup> /g)	$A_{BJHac}$ (m <sup>2</sup> /g)	$D_{aap}$ (Å)	$D_{aBJH}$ (Å)	$V_{spat}$ (cm <sup>3</sup> /g)	$V_{BJHacvp}$ (cm <sup>3</sup> /g)
M <sub>I</sub>	85.89	86.89	78.72	86.61	154.63	190.14	0.033	0.041
M <sub>II</sub>	41.06	45.89	72.71	23.46	167.49	369.49	0.019	0.021
M <sub>III</sub>	30.21	32.18	46.07	18.95	130.47	255.12	0.010	0.012
M <sub>IV</sub>	53.64	62.09	82.09	11.40	85.83	501.55	0.013	0.014
M <sub>V</sub>	117.85	119.11	12.86	106.24	205.91	235.70	0.061	0.071
M <sub>VI</sub>	59.02	60.70	69.00	58.18	382.65	394.76	0.058	0.057

$A_{sp}$  single-point surface area at  $P/P_0=0.2002$ ,  $A_{BET}$  BET surface area,  $A_{text}$   $t$  plot external surface area,  $A_{BJHac}$  BJH adsorption cumulative surface area of pores between 3.4- and 600-nm diameter,  $D_{aap}$  adsorption average pore diameter by BET (8  $V/A$ ),  $D_{aBJH}$  BJH adsorption average pore diameter,  $V_{spat}$  single point adsorption total pore volume of pores,  $V_{BJHacvp}$  BJH adsorption cumulative volume of pores

## Discussion

### Influence of nonpolar microemulsion phase

The change in nonpolar microemulsion phase density has no any effect on particle morphology. In most cases, spherical nanoparticles are obtained in reverse micelles where the surfactant-stabilized water nanodroplets play the role of nanoreactors. It was initially assumed that the nanodroplets could be used as templates to control the final size of the particles obtained in reverse micelles. However, later research has shown that there is no direct correlation between the droplet size and the particle size, although the droplet size does seem to have a great influence on the final particle size in many cases. Nevertheless, the combination of the droplet size with other parameters including intermicellar exchange rate, surfactant film flexibility, and reactant concentration can exert a delicate control over the final particle size [47]. For the tested M<sub>I</sub>, M<sub>II</sub>, and M<sub>III</sub> materials, spherical

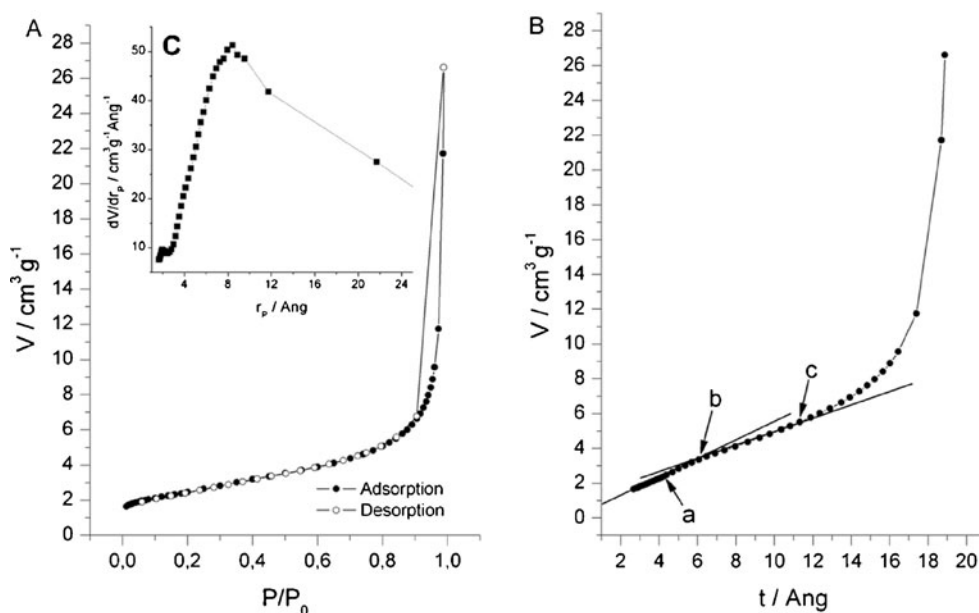
structures are obtained (Fig. 1). These facts are in accord with literature findings, which said that such characteristic only depends on water-to-surfactant ( $W_0$ ) and water-to-oil ratio [22, 25, 48]. For the specific case of AOT-stabilized microemulsions, it has been shown by neutron scattering that the  $W_0$  value determines the radius  $R$  of the spherical water droplet and a linear relation is found [49]:

$$R(\text{nm}) = 0.175 \times W_0 \quad (6)$$

In our studied systems,  $W_0=60$  and  $S_0=30$ , the theoretical value of the droplets obtained from Eq. (5) was 10.50 nm. This value is similar than those obtained for the average crystallite size ( $L$ ) determined by XRD line broadening technique using the Debye–Scherrer equation (Table 2).

From inspection of FE-SEM microphotographs (Fig. 1), an increase of particle agglomeration is seen, due to the increase of the templated microemulsion oil phase density. The microemulsion nonpolar phase density alters the microdroplet environment favoring microemulsion interdroplet attractive

**Fig. 7** **a** N<sub>2</sub> adsorption–desorption isotherm, **b**  $t$  plot, and **c** pore diameter distribution of  $M_I$ . The explanation of **a**, **b**, and **c** is in the text



interactions due to a reduction in solvent penetration into the interface [50, 51]. This fact would cause an increase of microdroplet association and the posterior particle agglomeration. As a result, there is a decrease in  $A_{\text{BET}}$  and in pore volume. The pore diameter is not affected by the variation of alkane density presumably because it directly depends on particle size and morphology.

The materials' phase composition (Fig. 3) is different from that of other  $\text{TiO}_2$  powder prepared by microemulsions method reported in the literature, for which pure  $\text{TiO}_2$  anatase was achieved [52]. The solvent effect on the crystalline phase of obtained materials is explained on basis of the preferential adsorption of the organic molecule on specific crystallite faces, which inhibits the growth of some planes and favors others [53, 54]. The presence of the organic residues provides nucleation sites for the rutile phase [55]. On the other hand, from XRD and FT-IR results, we can end that the  $\text{H}_2\text{O}$  and OH remaining after crystallization have a great effect on the anatase–rutile transition kinetics by breaking Ti–O bonds or by creating oxygen vacancies as it was previously found by Ha et al. [56].

#### Microemulsion temperature conditions effect

Usually, the works found in literature evaluated the variation of temperature in the hydrothermal and calcination [5, 53, 56] conditions and its effect in the final synthesized material morphology or in its crystallinity. Here, we found that small changes in the temperature during templated microemulsion preparation can cause similar effects. However, the variation of microemulsion preparation temperature conditions has no direct correlation with particle characteristics as the effect of nonpolar phase density has. Temperature effect is necessarily associated with a specific microemulsion system. So, for those materials templated with AOT/water/*n*-hexane, it can be seen that there is a variation of morphology and surface properties, while crystalline properties remain almost constant.

The formation of a microemulsion is an entropy-driven process. The enthalpy term is very small since only little work is required to form the water/oil interface due to the very small interfacial tension developing between the phases separated by the surfactant monolayer. As a consequence, the microscopic structure of the water and oil domains is strongly dependent on temperature. By Eicke et al. [57], it was first observed that the microemulsion electric conductivity increases drastically within a range of few degrees centigrade.

The temperature increase causes an augment of microdroplet interface flexibility. On the other hand, due to the dynamic character of the microemulsion, during the particle formation process, aggregates constantly collide. Both

mentioned facts favor the exchange rate of droplet content and the droplets coalescence. In some surfactant and oil phase conditions, the microemulsion transforms in a bicontinuous system; as a consequence, the obtained materials change from granular to a spongelike structure as we can appreciate for  $M_{\text{IV}}$  and  $M_{\text{VI}}$  materials in Fig. 2. Except for the water/AOT/*n*-hexane templated materials ( $M_{\text{I}}$  and  $M_{\text{IV}}$ ), all powders present an increase of  $A_{\text{BET}}$ , pore diameter, and pore volume with the augment of temperature. In the water/AOT/*n*-hexane microemulsion systems, the temperature increase caused a major droplet association, so the obtained material has a minor BET surface area, pore diameter, and pore volume.

The alteration of microemulsion (due to the temperature increase) probably changes the preferential adsorption of the organic and water molecules on specific crystallite faces and decreases the growth of rutile instead of anatase. So  $M_{\text{VI}}$  presents a 30 % reduction of rutile phase, while in  $M_{\text{V}}$ , it is completely absent.

#### Conclusions

Both microemulsion nonpolar phase density and temperature conditions have a great influence on the characteristic of the  $\text{TiO}_2$  nanopowders. A uniform  $\text{TiO}_2$  material composed of monodisperse spherical nanoparticles of  $R \approx 10$  nm was prepared by water/AOT/*n*-hexane reverse microemulsion at 30 °C. A change in microemulsion oil phase density leads to increased particle agglomeration and size while retaining almost constant spherical morphology. The alkane density also affects the material crystalline phase, favoring rutile growth instead of anatase. A brief increase in the microemulsion temperature condition causes an augment of particle agglomeration and in some systems a morphological change from granular to a bicontinuous structure. The fractal dimension of the  $\text{TiO}_2$  nanostructures tends to decrease as oil density increases. The change in morphology reduces the specific surface area of the material templated with AOT/water/*n*-hexane microemulsion, while for AOT/water/*n*-heptane and AOT/water/cyclohexane microemulsions, augments. For such systems, a high proportion of anatase phase is seen. Overall, this work shows the versatility of microemulsions to form a variety of structures due to the balance between their interfacial elasticity and temperature. Our results are expected to be useful to guide the design of nanostructures based on a simple, versatile, and rapid method of preparing nanomaterials with desirable properties for certain applications.

**Acknowledgments** The authors acknowledge the Xunta de Galicia (project no. 10PXIB206258PR) and Universidad Nacional del Sur, Concejo Nacional de Investigaciones Científicas y Técnicas de la República Argentina (CONICET, PIP-11220100100072).

## References

- Gratzel M (2001) Photoelectrochemical cells. *Nature* 414(6861):338–344
- Burda C, Chen X, Narayanan R, El-Sayed MA (2005) Chemistry and properties of nanocrystals of different shapes. *Chem Rev* 105(4):1025–1102. doi:10.1021/cr030063a
- Cozzoli PD, Pellegrino T, Manna L (2006) Synthesis, properties and perspectives of hybrid nanocrystal structures. *Chem Soc Rev* 35(11):1195–1208
- Stone V, Nowack B, Baun A, van den Brink N, von der Kammer F, Dusinska M, Handy R, Hankin S, Hassellöv M, Joner E, Fernandes TF (2010) Nanomaterials for environmental studies: classification, reference material issues, and strategies for physico-chemical characterisation. *Sci Total Environ* 408(7):1745–1754. doi:10.1016/j.scitotenv.2009.10.035
- Kim DS, Han SJ, Kwak S-Y (2007) Synthesis and photocatalytic activity of mesoporous TiO<sub>2</sub> with the surface area, crystallite size, and pore size. *J Colloid Interface Sci* 316(1):85–91. doi:10.1016/j.jcis.2007.07.037
- Zallen R, Moret MP (2006) The optical absorption edge of brookite TiO<sub>2</sub>. *Solid State Commun* 137(3):154–157. doi:10.1016/j.ssc.2005.10.024
- Lan Y, Gao XP, Zhu HY, Zheng ZF, Yan TY, Wu F, Ringer SP, Song DY (2005) Titanate nanotubes and nanorods prepared from rutile powder. *Adv Funct Mater* 15(8):1310–1318. doi:10.1002/adfm.200400353
- Holland BT, Blanford CF, Stein A (1998) Synthesis of macroporous minerals with highly ordered three-dimensional arrays of spheroidal voids. *Science* 281(5376):538–540. doi:10.1126/science.281.5376.538
- Meilert KT, Laub D, Kiwi J (2005) Photocatalytic self-cleaning of modified cotton textiles by TiO<sub>2</sub> clusters attached by chemical spacers. *J Mol Catal A Chem* 237(1–2):101–108. doi:10.1016/j.molcata.2005.03.040
- Mor GK, Oomman KV, Maggie P, Craig AG (2003) A self-cleaning, room-temperature titania-nanotube hydrogen gas sensor. *Sens Lett* 1(1):42–46. doi:10.1166/sl.2003.013
- Liu D, Zhang J, Han B, Chen J, Li Z, Shen D, Yang G (2003) Recovery of TiO<sub>2</sub> nanoparticles synthesized in reverse micelles by antisolvent CO<sub>2</sub>. *Colloids Surf, A Physicochem Eng Asp* 227(1–3):45–48. doi:10.1016/s0927-7757(03)00385-6
- The President's Council of Advisors on Science and Technology (2010). Report to the President and Congress on the third assessment of The National Nanotechnology Initiative. Executive Office of the President, White House Office of Science and Technology Policy. Washington, D.C.
- Shapira P, Wang J (2010) Follow the money. *Nature* 468(7324):627–628
- Cargnello M, Wieder NL, Montini T, Gorte RJ, Fornasiero P (2010) Synthesis of dispersible Pd@CeO<sub>2</sub> core-shell nanostructures by self-assembly. *J Am Chem Soc* 132(4):1402–1409. doi:10.1021/ja909131k
- Liu Z, Zhang X, Poyraz S, Surwade SP, Manohar SK (2010) Oxidative template for conducting polymer nanoclips. *J Am Chem Soc* 132(38):13158–13159. doi:10.1021/ja105966c
- Fernández-Leyes M, Verdinelli V, Hassan N, Ruso J, Pieroni O, Schulz P, Messina P (2012) Biomimetic formation of crystalline bone-like apatite layers on spongy materials templated by bile salts aggregates. *J Mater Sci* 47(6):2837–2844. doi:10.1007/s10853-011-6113-4
- Yoder NC, Kalsani V, Schuy S, Vogel R, Janshoff A, Kumar K (2007) Nanoscale patterning in mixed fluorocarbon/hydrocarbon phospholipid bilayers. *J Am Chem Soc* 129(29):9037–9043. doi:10.1021/ja0709501
- Mosquera V, Ruso JM, Prieto G, Sarmiento F (1996) Characterization of the interactions between lysozyme and *n*-alkyltrimethylammonium bromides by zeta potential measurements. *J Phys Chem* 100(41):16749–16753. doi:10.1021/jp960927e
- Sabín J, Prieto G, Messina PV, Ruso JM, Hidalgo-Alvarez R, Sarmiento F (2005) On the effect of Ca<sup>2+</sup> and La<sup>3+</sup> on the colloidal stability of liposomes. *Langmuir* 21(24):10968–10975. doi:10.1021/la051397t
- Ruso JM, Taboada P, Martínez-Landeira P, Prieto G, Sarmiento F (2001) A comparative study of the interaction between nafcillin and catalase by equilibrium dialysis and ζ-potential measurements. *J Phys Chem B* 105(13):2644–2648. doi:10.1021/jp003404m
- Lu C-H, Wu W-H, Kale RB (2008) Microemulsion-mediated hydrothermal synthesis of photocatalytic TiO<sub>2</sub> powders. *J Hazard Mater* 154(1–3):649–654. doi:10.1016/j.jhazmat.2007.10.074
- Deorsola FA, Vallauri D (2009) Study of the process parameters in the synthesis of TiO<sub>2</sub> nanospheres through reactive microemulsion precipitation. *Powder Technol* 190(3):304–309. doi:10.1016/j.powtec.2008.08.009
- Hassan N, Verdinelli V, Ruso JM, Messina PV (2011) Mimicking natural fibrous structures of opals by means of a microemulsion-mediated hydrothermal method. *Langmuir* 27(14):8905–8912. doi:10.1021/la201555f
- Hassan N, Verdinelli V, Ruso JM, Messina PV (2012) Assessing structure and dynamics of fibrinogen films on silicon nanofibers: towards hemocompatibility devices. *Soft Matter* 8(24):2582–2592
- Hellweg T (2002) Phase structures of microemulsions. *Curr Opin Colloid Interface Sci* 7(1–2):50–56. doi:10.1016/s1359-0294(02)00004-3
- Pileni MP (1997) Nanosized particles made in colloidal assemblies. *Langmuir* 13(13):3266–3276. doi:10.1021/la960319q
- Pileni MP (2001) Mesostructured fluids in oil-rich regions: structural and templating approaches. *Langmuir* 17(24):7476–7486. doi:10.1021/la010538y
- Shevachman M, Shani A, Garti N (2004) Formation and investigation of microemulsions based on jojoba oil and nonionic surfactants. *J Am Oil Chem Soc* 81(12):1143–1152. doi:10.1007/s11746-004-1032-2
- Schlicht L, Spilgies JH, Runge F, Lipgens S, Boye S, Schübel D, Ilgenfritz G (1996) Temperature-, electric field- and solute-induced percolation in water-in-oil microemulsions. *Biophys Chem* 58(1–2):39–52. doi:10.1016/0301-4622(95)00084-4
- Van Dijk MA, Joosten JGH, Levine YK, Bedeaux D (1989) Dielectric study of temperature-dependent aerosol OT/water/isooctane microemulsion structure. *J Phys Chem* 93(6):2506–2512. doi:10.1021/j100343a054
- Moha-Ouchane M, Peyrelasse J, Boned C (1987) Percolation transition in microemulsions: effect of water-surfactant ratio, temperature, and salinity. *Phys Rev A* 35(7):3027–3032
- Alexandridis P, Holzwarth JF, Hatton TA (1993) Interfacial dynamics of water-in-oil microemulsion droplets: determination of the bending modulus using iodine laser temperature jump. *Langmuir* 9(8):2045–2052. doi:10.1021/la00032a024
- Alexandridis P, Holzwarth JF, Hatton TA (1995) Thermodynamics of droplet clustering in percolating AOT water-in-oil microemulsions. *J Phys Chem* 99(20):8222–8232. doi:10.1021/j100020a054
- Giorgilli A, Casati D, Sironi L, Galgani L (1986) An efficient procedure to compute fractal dimensions by box counting. *Phys Lett A* 115(5):202–206. doi:10.1016/0375-9601(86)90465-2
- Foroutan-pour K, Dutilleul P, Smith DL (1999) Advances in the implementation of the box-counting method of fractal dimension estimation. *Appl Math Comput* 105(2–3):195–210. doi:10.1016/s0096-3003(98)10096-6
- Bau S, Witschger O, Gensdarmes F, Rastoix O, Thomas D (2010) A TEM-based method as an alternative to the BET method for

- measuring off-line the specific surface area of nanoaerosols. *Powder Technol* 200(3):190–201. doi:10.1016/j.powtec.2010.02.023
37. Ibaseta N, Biscans B (2010) Fractal dimension of fumed silica: comparison of light scattering and electron microscope methods. *Powder Technol* 203(2):206–210. doi:10.1016/j.powtec.2010.05.010
38. Chang C-L, Fogler HS (1997) Controlled formation of silica particles from tetraethyl orthosilicate in nonionic water-in-oil microemulsions. *Langmuir* 13(13):3295–3307. doi:10.1021/la961062z
39. Mohapatra P, Mishra T, Parida KM (2006) Effect of microemulsion composition on textural and photocatalytic activity of titania nanomaterial. *Appl Catal Gen* 310:183–189. doi:10.1016/j.apcata.2006.05.041
40. Spurr RA, Myers H (1957) Quantitative analysis of anatase-rutile mixtures with an X-ray diffractometer. *Anal Chem* 29(5):760–762. doi:10.1021/ac60125a006
41. Periyat P, McCormack DE, Hinder SJ, Pillai SC (2009) One-pot synthesis of anionic (nitrogen) and cationic (sulfur) codoped high-temperature stable, visible light active, anatase photocatalysts. *J Phys Chem C* 113(8):3246–3253. doi:10.1021/jp808444y
42. Naono H, Hakuman M, Shiono T (1997) Analysis of nitrogen adsorption isotherms for a series of porous silicas with uniform and cylindrical pores: a new method of calculating pore size distribution of pore radius 1–2 nm. *J Colloid Interface Sci* 186(2):360–368. doi:10.1006/jcis.1996.4677
43. Lippens BC, Linsen BG, Boer JH (1964) Studies on pore systems in catalysts I. The adsorption of nitrogen; apparatus and calculation. *J Catal* 3(1):32–37. doi:10.1016/0021-9517(64)90089-2
44. Barrett EP, Joyner LG, Halenda PP (1951) The determination of pore volume and area distributions in porous substances. I. Computations from nitrogen isotherms. *J Am Chem Soc* 73(1):373–380. doi:10.1021/ja01145a126
45. de Boer JH, Lippens BC, Linsen BG, Broekhoff JCP, van den Heuvel A, Osinga TJ (1966) Thet-curve of multimolecular N<sub>2</sub>-adsorption. *J Colloid Interface Sci* 21(4):405–414. doi:10.1016/0095-8522(66)90006-7
46. Halsey G (1948) Physical adsorption on non-uniform surfaces. *J Chem Phys* 16(10):931–937
47. Limin Q (2007) Synthesis of inorganic nanostructures in reverse micelles. In: *Encyclopedia of surface and colloid Science*, 2nd edn. Taylor & Francis, New York, pp 6183–6207. doi:10.1081/E-ESCS-120023694
48. Yadav OP, Palmqvist A, Cruise N, Holmberg K (2003) Synthesis of platinum nanoparticles in microemulsions and their catalytic activity for the oxidation of carbon monoxide. *Colloids Surf, A Physicochem Eng Asp* 221(1–3):131–134. doi:10.1016/s0927-7757(03)00141-9
49. Nicholson JD, Clarke LH (1984) In: Mittal KL, Lindman B (eds) *Surfactants in solution*. New York, Plenum
50. Hamilton RT, Billman JF, Kaler EW (1990) Measurements of interdroplet attractions and the onset of percolation in water-in-oil microemulsions. *Langmuir* 6(11):1696–1700. doi:10.1021/la00101a013
51. Johannsson R, Almgren M, Alsins J (1991) Fluorescence and phosphorescence study of AOT/water/alkane systems in the L2 reversed micellar phase. *J Phys Chem* 95(9):3819–3823. doi:10.1021/j100162a070
52. Moriguchi I, Hidaka R, Yamada H, Kudo T (2005) Li-intercalation property of mesoporous anatase-TiO<sub>2</sub> synthesized by bicontinuous microemulsion-aided process. *Solid State Ionics* 176(31–34):2361–2366. doi:10.1016/j.ssi.2005.02.029
53. Zhao X, Yu J, Cheng B, Zhang Q (2005) Crystallization of lead sulfide in the presence of poly(methacrylic acid) or/and cetyltrimethylammonium bromide. *Colloids Surf, A Physicochem Eng Asp* 268(1–3):78–84. doi:10.1016/j.colsurfa.2005.05.063
54. Bujan M, Sikirić M, Filipović-Vinceković N, Vdović N, Garti N, Füredi-Milhofer H (2001) Effect of anionic surfactants on crystal growth of calcium hydrogen phosphate dihydrate. *Langmuir* 17(21):6461–6470. doi:10.1021/la0107190
55. Mercera PDL, Van Ommen JG, Doesburg EBM, Burggraaf AJ, Ross JRH (1992) Influence of ethanol washing of the hydrous precursor on the textural and structural properties of zirconia. *J Mater Sci* 27(18):4890–4898. doi:10.1007/bf01105251
56. Ha PS, Youn H-J, Jung HS, Hong KS, Park YH, Ko KH (2000) Anatase–rutile transition of precipitated titanium oxide with alcohol rinsing. *J Colloid Interface Sci* 223(1):16–20. doi:10.1006/jcis.1999.6607
57. Eicke HF, Borkovec M, Das-Gupta B (1989) Conductivity of water-in-oil microemulsions: a quantitative charge fluctuation model. *J Phys Chem* 93(1):314–317. doi:10.1021/j100338a062